Am J Physiol Cell Physiol 326: C400–C413, 2024.
First published December 18, 2023; doi:10.1152/ajpcell.00394.2023

american physiological society

AMERICAN JOURNAL OF PHYSIOLOGY
CELL PHYSIOLOGY

RESEARCH ARTICLE

Decoding Fibrosis

OTUD6A in tubular epithelial cells mediates angiotensin II-induced kidney injury by targeting STAT3

Xiaoyu Sun,[1,2,3]* Shuhong Chen,[2]* Ying Zhao,[4] Tong Wu,[2] Zheyu Zhao,[2] Wu Luo,[4] Jibo Han,[4] Zimin Fang,[4] Bozhi Ye,[4] Gang Cao,[5] Shengbin Huang,[2,3] and Guang Liang[1,4]

[1]*Affiliated Yongkang First People's Hospital and School of Pharmacy, Hangzhou Medical College, Hangzhou, People's Republic of China;* [2]*Institute of Stomatology, School and Hospital of Stomatology, Wenzhou Medical University, Wenzhou, People's Republic of China;* [3]*Department of Periodontics and Prosthodontics, School and Hospital of Stomatology, Wenzhou Medical University, Wenzhou, People's Republic of China;* [4]*Chemical Biology Research Center, School of Pharmaceutical Sciences, Wenzhou Medical University, Wenzhou, People's Republic of China; and* [5]*School of Pharmacy, Zhejiang Chinese Medical University, Hangzhou, People's Republic of China*

Abstract

Kidney fibrosis is a prominent pathological feature of hypertensive kidney diseases (HKD). Recent studies have highlighted the role of ubiquitinating/deubiquitinating protein modification in kidney pathophysiology. Ovarian tumor domain-containing protein 6 A (OTUD6A) is a deubiquitinating enzyme involved in tumor progression. However, its role in kidney pathophysiology remains elusive. We aimed to investigate the role and underlying mechanism of OTUD6A during kidney fibrosis in HKD. The results revealed higher OTUD6A expression in kidney tissues of nephropathy patients and mice with chronic angiotensin II (Ang II) administration than that from the control ones. OTUD6A was mainly located in tubular epithelial cells. Moreover, OTUD6A deficiency significantly protected mice against Ang II-induced kidney dysfunction and fibrosis. Also, knocking OTUD6A down suppressed Ang II-induced fibrosis in cultured tubular epithelial cells, whereas overexpression of OTUD6A enhanced fibrogenic responses. Mechanistically, OTUD6A bounded to signal transducer and activator of transcription 3 (STAT3) and removed K63-linked-ubiquitin chains to promote STAT3 phosphorylation at tyrosine 705 position and nuclear translocation, which then induced profibrotic gene transcription in epithelial cells. These studies identified STAT3 as a direct substrate of OTUD6A and highlighted the pivotal role of OTUD6A in Ang II-induced kidney injury, indicating OTUD6A as a potential therapeutic target for HKD.

NEW & NOTEWORTHY Ovarian tumor domain-containing protein 6 A (OTUD6A) knockout mice are protected against angiotensin II-induced kidney dysfunction and fibrosis. OTUD6A promotes pathological kidney remodeling and dysfunction by deubiquitinating signal transducer and activator of transcription 3 (STAT3). OTUD6A binds to and removes K63-linked-ubiquitin chains of STAT3 to promote its phosphorylation and activation, and subsequently enhances kidney fibrosis.

deubiquitinase; hypertensive kidney diseases; OTUD6A; STAT3; tubular epithelial cells

INTRODUCTION

Hypertension negatively affects 1 billion people worldwide. The kidney is the primary organ of hypertension-induced targeted injuries. Hypertensive kidney disease (HKD) is a highly prevalent disease affecting more than 10% of people worldwide and is associated with severe morbidity and mortality (1). Kidney fibrosis is a prominent pathological feature and the main prognostic factor of HKD. Alleviating kidney fibrosis has potential clinical significance for kidney diseases; however, currently, effective therapies are limited (2). Understanding the molecular mechanisms underlying kidney fibrosis offers novel insights into developing new therapeutic avenues for HKD.

A considerable amount of clinical and experimental studies implicate a fundamental role of renin-angiotensin (Ang) system (RAS) in driving hypertensive renal fibrosis (3). Angiotensin II (Ang II), the most crucial effector in the RAS, is upregulated in various renal fibrosis models. Inhibitors of Ang-converting enzyme are used as first-line medications to prevent hypertensive renal fibrosis (4). Identifying regulatory molecules underlying Ang II-induced kidney injury carries significant clinical value. The pathophysiology of kidney fibrosis is multifactorial, of which protein modification is

*X. Sun and S. Chen contributed equally to this article.
Correspondence: S. Huang (huangsb003@wmu.edu.cn); L. Guang (wzmcliangguang@163.com).
Submitted 21 August 2023 / Revised 4 December 2023 / Accepted 4 December 2023

crucial in regulating kidney homeostasis and function (5). The ubiquitin-proteasome system (UPS) is a pivotal intracellular and nonlysosomal protein degradation system promoted by ubiquitinating enzymes and counter-controlled by deubiquitinating enzymes (DUBs; 6). DUBs are proteases that regulate protein turnover by detaching ubiquitin from proteins and are emerging therapeutic targets for various diseases (7). They are classified into five families: ubiquitin-specific protease (USP), ubiquitin carboxyl-terminal hydrolase (UCH), JAB1/MPN/MOV34 (JAMM), ovarian tumor protease (OTU), and Machado-Joseph (MJD; 8). Researches on DUBs in kidney remolding are limited. Only recently, dysregulated DUBs, purely from the USP family, such as USP7, USP22, USP25, and USP28, were linked to kidney injury (9–12). However, most substrates and pathways modulated by DUBs from the other families except USP remain largely elusive, hindering efforts to prioritize therapeutic targets for kidney diseases. Ovarian tumor deubiquitinase 6 A (OTUD6A) is a newly identified deubiquitinase from the out family. A few studies revealed the role of OTUD6A in cancer progression and inflammatory bowel disease (13–15). To date, the potential function of OTUD6A in kidney homeostasis and diseases remains elusive.

Our study provides the first direct evidence of the upregulated level of OTUD6A in kidney tissues and cells challenged by Ang II. We used OTUD6A knockout (*OTUD6A*$^{-/-}$) mice and revealed that OTUD6A deficiency attenuated Ang II-mediated kidney dysfunction and fibrosis. The detailed mechanistic studies demonstrated that OTUD6A bounded to signal transducer and activator of transcription 3 (STAT3) and cleaved K63-linked ubiquitin chains to enhance STAT3 phosphorylation at tyrosine 705 and nuclear translocation; thereby, STAT3 was activated to elicit fibrosis in epithelial cells. These studies indicate that OTUD6A plays a vital role in kidney fibrosis, and the blockade of OTUD6A represents a potential therapeutic strategy for HKD.

MATERIALS AND METHODS

Reagents

Ang II (No. HY-13948) and stattic (No. HY-13818) were obtained from Med Chem Express (New Jersey). Small interfering RNA {siRNA, [small interfering RNA-ovarian tumor domain-containing protein 6A (si-OTUD6A) and small interfering RNA-negative control (si-NC)]} was purchased from Ribobio (Guangzhou, PR China; Supplemental Table S1). Plasmids (Flag-OTUD6A, His-STAT3, HA-Ub, HA-K48, HA-K63) were from Genechem (Shanghai, PR China). Antibodies against STAT3 (No. sc-8019, 1:1,000), AQP1 (aquaporin 1; No. sc-25287, 1:200), Ub (Ubiquitin; No. sc-8017, 1:200), and WT1 (Wilms tumor 1; No. sc-7385, 1:1,000) were purchased from Santa Cruz Biotech (Texas). The antibody against p-STAT3 (phosphorylated STAT3) (Y705; No. AP0705, 1:1,000) was from Abclonal Technology (Boston). Antibodies against collagen type 1 (Col-1; No. ab138492, Abcam, 1:1,000), alpha-smooth muscle actin (α-SMA; No. 67735-1-Ig, Proteintech, 1:1,000), and Lamin B1 (No. ab133741, Abcam, 1:1,000) were from Abcam (Cambridge, UK). Antibodies against OTUD6A (No. 24486-1-AP, 1:1,000), Desmin (No. MA5-13259, Invitrogen Life Technology, 1:200) was purchased. IgG-Tag (No. 30000-0-AP, 1:1,000), FLAG-Tag (No. 20543-1-AP, 1:1,000), HA-Tag (No. 51064-2-AP, 1:1,000) were from Proteintech Biotechnology (PR China). NcmECL Ultra (No. P10010) was from NCM Biotech (Suzhou, PR China). Antibodies against β-actin (No. MA1-140, 1:1,000) were from Invitrogen Life Technology (Carlsbad, CA). The hematoxylin-eosin staining (H&E) assay kit (No. G1120), periodic acid-Schiff (PAS) kit (No. G1280), picrosirius red (No. S8060), and Masson's trichrome stain kit (No. G1340) were from Solarbio Life Sciences (Beijing, PR China). 4',6-diamidino-2-phenylindole (DAPI; No. 36308ES11) was from Yeasen, Shanghai, China. The detailed information for antibodies is shown in Supplemental Table S2.

Human Kidney Samples

Six patients with primary IgA nephropathy were obtained from the Renal Disease Center of the First Affiliated Hospital of Zhejiang Medical University. According to the 2016 Oxford classification (16), the patients were divided into the T0 group (interstitial fibrosis 0%–25%) and the T1 group (interstitial fibrosis >25%). Paraffin sections were obtained for immunohistochemical staining. This experiment was approved by the Ethics Committee in Clinical Research (ECCR) of the First Affiliated Hospital of Zhejiang University to use clinical biopsy specimens (Approval No.: 2023IIT No. 27), and informed consent was obtained from the patients. All studies followed the Declaration of Helsinki of 1975, amended in 2008 (17). The patient information is shown in Supplemental Table S3.

Animal Experiments

The whole body *OTUD6A*$^{-/-}$ mice in the C57BL/6J background were provided by Professor Fuping You (Peking University, Beijing, PR China). In the present study, heterozygous OTUD6A mice were hybridized to produce homozygous *OTUD6A*$^{-/-}$ and wild-type (WT) littermate animals. *OTUD6A*$^{-/-}$ and WT mice were maintained in a specific pathogen free (SPF) environment with 12 h of light and adequate access to food and water. The mouse feeding and experimental procedures received approval from the Ethics Examination and Approval Committee of the Animal Experimental Center of The First Affiliated Hospital of Wenzhou Medical University (WYDW-2021-0073). To identify the mouse genotypes, cDNA was extracted from the mouse tail, and primers for the *OTUD6A*$^{-/-}$ and WT type were used to identify mouse genotypes. Detailed experimental procedures used in amplification and the sequence of the primers are shown in Supplemental Table S4.

For Ang II-induced kidney fibrosis model, 12 *OTUD6A*$^{-/-}$ and 12 WT mice aged 6–8 wk were randomized into four groups, with six mice in each group. We adopted all animal experiments in male mice to eliminate the possible effects of estrogen and testosterone on kidney fibrosis upon the Ang II challenge. The mice were injected with Ang II (1 μg/kg/min) or saline with a subcutaneously implanted osmotic minipump in the back of the mouse (No. Alzet MODEL 1004) for 4 wk (18). The incision of the mice was observed daily. The blood pressure was measured and recorded every 3 days. The model was confirmed to be successful when the systolic blood pressure was greater than 150 mmHg and maintained for 4 wk. Then all mice were euthanized under

anesthesia, and their serum and kidney tissues were extracted for further examination. Serum kidney function biomarkers, including blood urine nitrogen and serum creatinine, were examined by commercial kits (Jian Cheng Bioengineering Institute, Nanjing, PR China).

Histological Analysis and Immunohistochemistry

The kidney tissue was fixed by 4% formaldehyde, dehydrated, transparent, and embedded with paraffin. Finally, the kidney tissue was cut into 6 μM thick samples for subsequent experiments. The slices were stained with H&E, PAS, picrosirius red, and Masson's trichrome, according to the manufacturer's specifications. Paraffin sections were stained with 0.1% Sirius red and 1.3% picric acid-saturated aqueous solution to assess type IV collagen deposition.

The sections were subjected to antigen retrieval in 0.01 mol/L citrate buffer for immunohistochemistry and blocked with 3% H_2O_2. Then the sections were stained with anti-OTUD6A (1:400), anti-p-STAT3 (1:200), and anti-α-SMA (1:400). Slides were washed with PBS for three times and incubated with secondary antibody (PV9000, ZSGB-BIO, Beijing, PR China) at room temperature for 0.5 h. Next, diaminobenzidine generated color and counterstained the sections with Mayer's hematoxylin. Images were taken with a digital camera (Nikon, Japan), and the percentage of positive area per unit was evaluated.

Regarding the statistical analysis of picrosirius red, Masson staining sections, and immunohistochemistry sections, at least four fields from each sample were obtained at ×200 magnifications, respectively. The positive areas were analyzed using ImageJ-Fiji (19). Large blood vessels were excluded from the analysis of the picrosirius red positive area using Gimp 2.10.10 (GNU Image Manipulation Program; 20). The percentage of the tissues consisting of interstitial collagen was calculated as the ratio of picrosirius red positively stained area over the total tissue area. Regarding the immunohistochemistry staining, the percentage of positive area was calculated as the ratio of positively stained area over the total tissue area.

Cell Culture and Transfection

The NRK-52E (normal rat kidney epithelial cell) cells were from the Shanghai Institute of Biochemistry and Cell Biology (Shanghai, PR China), and cultured in Dulbecco's Modified Eagle's medium (DMEM) that contains 10% fetal bovine serum, 100 U/mL penicillin, and 100 U/mL streptomycin. According to the previous reports, NRK-52E cells were challenged with 1 μM Ang II to develop in vitro HKD model (21–23). The mouse embryonic fibroblast cells (NIH/3T3) cells were from the Shanghai Institute of Biochemistry and Cell Biology (Shanghai, PR China). A DMEM medium with 4.5 g/L glucose containing 10% fetal bovine serum and 1% penicillin/streptomycin was used to culture the cells. When the cell density in the six-well plate reached 60%, we transfected 1 μg plasmid using Opti-MEMTM medium (No. 31985070, Thermo Fisher Scientific, Germany) containing 2 μL Lipofectamine 3000 and 2 μL P3000 (No. L3000-015, Thermo Fisher Scientific, Germany). siRNA (50 nM) were transfected by using Opti-MEMTM medium containing 2 μL Lipofectamine 3000. The cells were transfected 24 h later for subsequent experiments.

Immunofluorescence Staining

The NRK-52E cells grown on glass coverslips were stimulated with or without Ang II for immunofluorescence experiments. Then the cells were fixed by methanol and blocked with 5% bovine serum albumin. The cells were incubated with antibodies at 4°C overnight and further with secondary antibodies (No. ab150077, Abcam, 1:200, and No. CL594-10594, Proteintech, 1:200) for 2 h at room temperature. Finally, the cells were counterstained with DAPI and imaged by the Nikon microscope imaging system.

Western Blotting and Coimmunoprecipitation

Total proteins were isolated by radioimmunoprecipitation (RIPA) lysis buffer (No. P0013C, Beyotime Biotechnology). Then the concentration of proteins was determined with equal amounts of protein separated by sodium dodecyl sulfate-polyacrylamide gel electrophoresis and transferred to PVDF membranes. The membranes were blocked by 5% nonfat dry milk and incubated with primary antibody overnight at 4°C. Then, the membrane was incubated with the horseradish peroxidase (HRP)-conjugated anti-mouse secondary antibody (No. SA00001-1, Proteintech, 1:2,000) and rabbit secondary antibody (No. SA00001-2, Proteintech, 1:2,000) at room temperature. Finally, protein content was determined using the Bio-Rad protein assay (Bio-Rad, Munich, Germany). The signals in the membrane were revealed by the electrochemiluminescence reagent. The intensity analysis was performed by the ImageJ-Fiji and normalized to β-actin, STAT3, or Lamin B1.

For coimmunoprecipitation (Co-IP), proteins were extracted from animal kidney tissue (10 mg) and primary NRK-52E cell (1×10^7) samples with 0.4 mL RIPA buffer. Then, 200 μL protein lysate (1 mg/mL) was treated with 30 μL protein A + G agarose beads (No. P2012, Beyotime Biotechnology, PR China) on a vibrator at 4°C for 1 h. The supernatant was transferred to the new tube to remove proteins bound explicitly to magnetic beads after centrifugation at 4°C for 10 min. A portion of the lysate was retained as an input sample. The corresponding primary antibody (1 μg) was then added to the lysate and incubated overnight on a vibrator at 4°C. Subsequently, 30 μL protein A + G agarose beads were added to the lysate and incubated at 4°C for 2 h. The supernatant of protein lysate was discarded after centrifugation at 1,500 *g* for 5 min. The magnetic bead mixture obtained in the previous step was washed with PBS for five times, then the magnetic bead mixture was treated with Tris-glycine sample loading buffer containing 2× sodium dodecyl sulfate (SDS), followed by a heat treatment at 100°C for 10 min. Finally, after centrifugation at 14,000 *g* for 1 min, the supernatant was used for the subsequent Western blot procedure.

Extraction of Cytoplasmic and Nuclear Proteins

NRK-52E cells were prepared in 10 cm dishes for extraction of the cytoplasmic and nuclear proteins. Nuclear and cytoplasmic proteins were isolated using NE-PER nuclear and cytoplasmic extraction reagents (No. P0028, Beyotime Biotechnology, PR China), according to the manufacturer's protocol.

Real-Time Quantitative PCR

Total RNA from kidney tissue and NRK-52E cells were isolated and purified with TRIzol reagent (No. R401-01, Vazyme, PR China) and reverse-transcribed to cDNA using PrimeScript RT reagent kit (No. DRR037A, Takara, Japan). Quantitative polymerase chain reaction (PCR) was carried out with SYBR Green reagent kits (No. DRR037A, Takara, Japan). PCR was subjected to 30 cycles, including 1 min each for 94°C (denaturation), 60°C (annealing), and 72°C (elongation), and finally

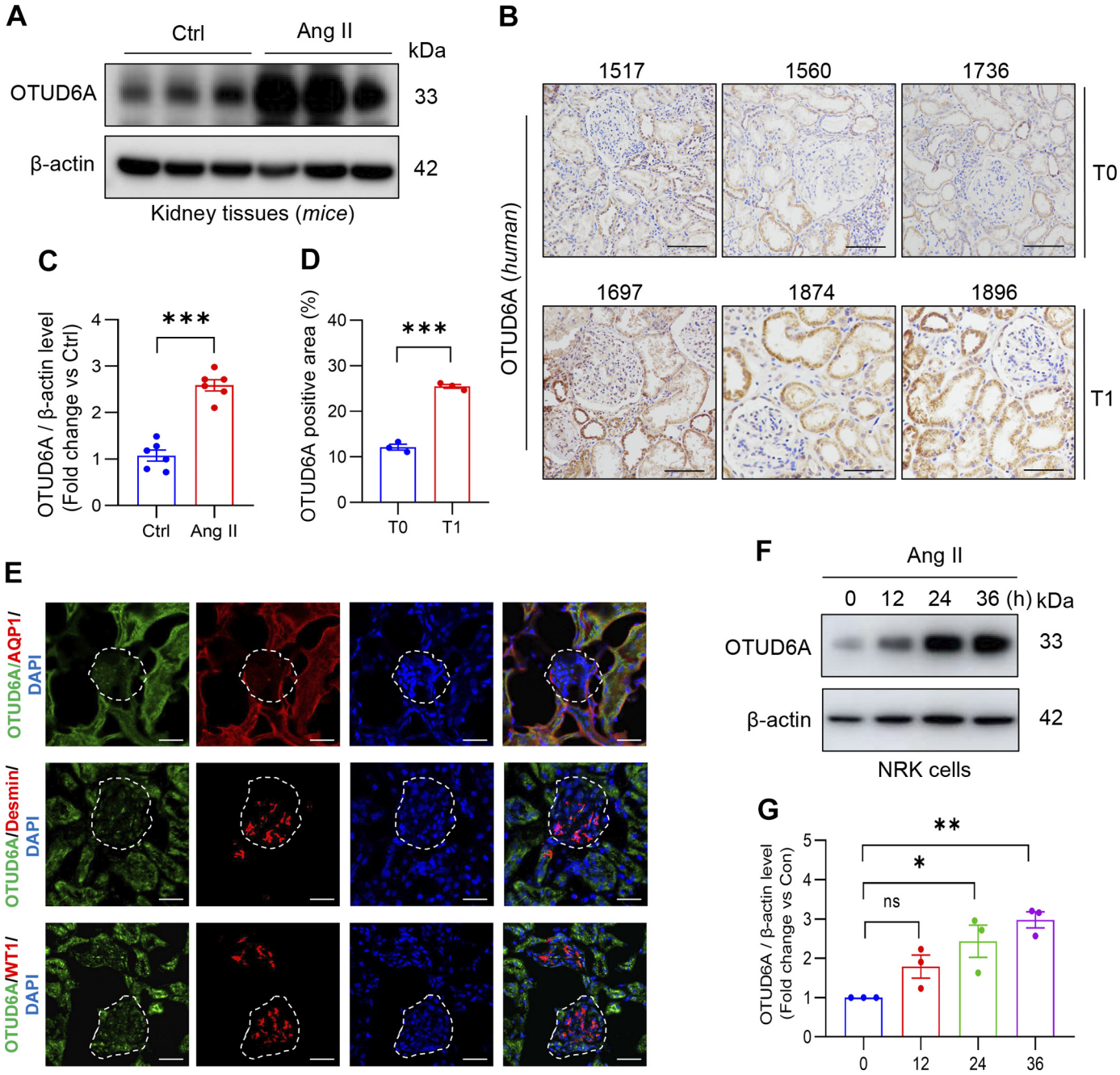

Figure 1. OTUD6A was upregulated in kidney tissues of both mice challenged with Ang II and patients with nephropathy as compared with the control ones. *A*: representative immunoblots for OTUD6A levels in Ctrl and Ang II-infused kidney tissues. *B*: representative immunohistochemical staining of OTUD6A in kidney biopsy samples obtained from patients with nephropathy of different tubular atrophy/interstitial fibrosis (T0 and T1) (scale bar = 50 μm). C: quantification of the protein levels of OTUD6A in mice kidney tissues (Normalized to β-actin; $n = 6$). *D*: quantification of OTUD6A protein level in kidney biopsy samples obtained from patients with nephropathy of different tubular atrophy/interstitial fibrosis (T0 and T1; $n = 3$). *E*: immunofluorescent staining of mouse kidney samples for OTUD6A (green) and markers of kidney epithelial cells [AQP1 (aquaporin-1); red], and mesangial cells and injured podocytes (desmin; red), and podocytes [WT1 (Wilms tumor-1); red]. Slides were counterstained with 4′,6-diamidino-2-phenylindole (DAPI; scale bar = 25 μm). *F* and *G*: representative immunoblots and quantitative analysis for OTUD6A protein levels in primary NRK-52E cells challenged by Ang II (Normalized to β-actin; $n = 3$). Ns, not significant, $^{*}P < 0.05$, $^{**}P < 0.01$, and $^{***}P < 0.001$. Ang II, angiotensin II; Ctrl, control; NRK cell, normal rat kidney epithelial cell; OTUD6A, ovarian tumor domain-containing protein 6 A.

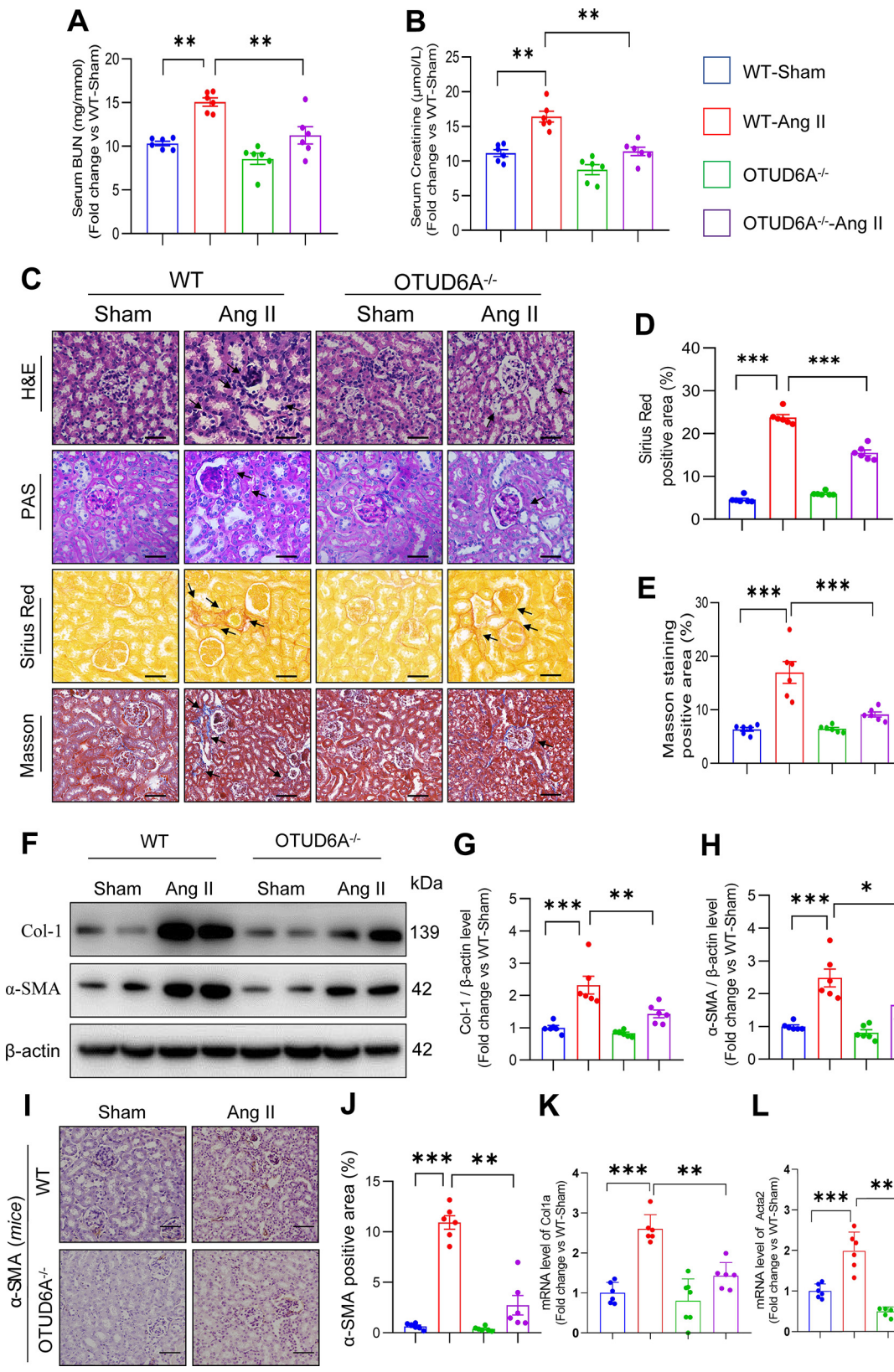

AJP-Cell Physiol • doi:10.1152/ajpcell.00394.2023 • www.ajpcell.org

extension at 72°C for 10 min. Primers were from Sangon Biotech (Shanghai, PR China), as shown in Supplemental Table S4.

Liquid Chromatograph-Mass Spectrometer Analysis

NIH/3T3 cells were transfected with plasmids expressing Flag-tagged OTUD6A. After 24 h, the cells were lysed with a Co-IP lysis buffer. The samples were then enriched with Flag antibody and protein A + G agarose beads at 4°C overnight before being eluted with PBS three times. Next, the samples were subjected to SDS-PAGE gel and Coomassie blue staining. The excised gel segments were subjected to liquid chromatograph-mass spectrometer (LC-MS/MS) and analyzed by H-wayen Biomedical Science and Technology Co Ltd (Shanghai, PR China).

Statistical Analysis

Data are presented as the means ± standard deviation (SD) and analyzed using GraphPad Pro Prism 8.0 (GraphPad, San Diego, CA; 24). The student's *t* test was adopted to analyze the difference between two groups. Furthermore, the data were analyzed by one-way ANOVA to compare the difference between multiple groups. *P* values less than 0.05 were statistically significant.

RESULTS

OTUD6A Expression Was Elevated in Kidney Tissues of Mice Challenged with Ang II and Patients with Kidney Fibrosis

We used the well-established Ang II-induced hypertension mice model to evaluate the role of OTUD6A. The results revealed that as compared with mice in the control group, mice administered with Ang II for 4 wk had elevated levels of OTUD6A in kidney tissues (Fig. 1*A*). To further evaluate the possible role of OTUD6A in renal fibrosis, we analyzed the OTUD6A level in fibrotic kidney samples from patients with nephropathy. The patients were divided into the T0 group (interstitial fibrosis 0%–25%) and the T1 group (interstitial fibrosis >25%) according to the 2016 Oxford classification. The immunostaining results demonstrated that the OTUD6A level was higher in the T1 group than in the T0 group. These data indicated a potential link between OTUD6A and tubular atrophy/interstitial fibrosis levels in human kidney tissues (Fig. 1*B*). Quantification of OTUD6A expression further confirmed increased OTUD6A protein level in kidney tissues of mice infused with Ang II and patients with nephropathy as compared with the controls (Fig. 1, *C* and *D*).

To identify the source of OTUD6A in the kidney tissues, we used AQP1 to mark kidney epithelial cells, Desmin to mark mesangial cells and injured podocytes, and WT1 to label podocytes. Our findings revealed that OTUD6A immunoreactivity mainly colocalized to AQP1-expressing cells rather than Desmin and WT1-expressing cells. Therefore, the kidney tubular cells were the primary source of increased OTUD6A in kidney tissues following Ang II administration (Fig. 1*E*). We further confirmed these findings in normal rat kidney (NRK)-52E kidney tubular epithelial cells. Immunoblotting showed that OTUD6A levels were significantly increased following Ang II challenge in NRK-52E cells (Fig. 1, *F* and *G*; Supplemental Fig. S1). These results suggested that elevated OTUD6A expression in kidney tubular cells correlated with local kidney injuries in humans and mice, potentially related to kidney remodeling.

OTUD6A Deficiency Protected Mice against Ang II-Induced Kidney Dysfunction and Fibrosis

To explore the role of OTUD6A in kidney dysfunction, we utilized *OTUD6A*$^{-/-}$ mice. The immunostaining staining also confirmed that mice administered with Ang II presented elevated OTUD6A level in kidney tissues (Supplemental Fig. S2). WT and *OTUD6A*$^{-/-}$ mice were administrated with saline or Ang II for 4 wk. Both WT and OTUD6A$^{-/-}$ mice challenged with Ang II showed increased blood pressure compared with saline-infused mice, suggesting that blood pressure in response to Ang II was not affected by OTUD6A deficiency (Supplemental Fig. S3). OTUD6A deficiency prevented Ang II-induced kidney dysfunction, as evidenced by decreased serum creatinine ratio and blood urea nitrogen levels (Fig. 2, *A* and *B*).

Gross examination of kidney tissues from mice further showed that OTUD6A deficiency protected mice against Ang II-induced kidney fibrosis. H&E staining confirmed that Ang II-induced tubular injury in WT mice was reflected by tubular dilation, epithelia flattening, and tubular loss, which were attenuated in *OTUD6A*$^{-/-}$ mice. PAS staining revealed that Ang II increased mesangial cell proliferation and thickening of basement membranes, which was attenuated by OTUD6A knockout. Sirius red and Masson's trichrome staining further showed enhanced collagen deposition and fibrosis in kidney tissues upon Ang II challenge in mice, which were suppressed in *OTUD6A*$^{-/-}$ mice (Fig. 2, *C*–*E*). Consistent with the histological examination, levels of fibrosis-associated factors kidney collagen 1 (Col-1) and alpha-smooth muscle actin (α-SMA) following Ang II-infusion were

Figure 2. OTUD6A deficiency attenuated Ang II-induced kidney dysfunction and fibrosis. WT and *OTUD6A*$^{-/-}$ mice were infused with saline (Sham) or Ang II for 4 wk. Male mice aged 6–8 wk were randomized into four groups, with six mice in each group. *A* and *B*: measures of kidney function showing BUN and serum creatinine ratio level ($n = 6$). *C*: fibrosis in kidney tissues was determined by staining with hematoxylin-eosin (H&E), periodic acid-Schiff (PAS), Sirius red, and Masson in sections of kidney (scale bar, 50 μm for H&E and PAS, Sirius red, and Masson staining). Black arrows indicating the collagen deposition and fibrosis. *D* and *E*: quantification of Sirius red and Masson staining scores ($n = 6$). *F*: representative immunoblots of Col-1 and α-SMA in kidney tissues from WT or *OTUD6A*$^{-/-}$ mice under Ang II treatment. *G* and *H*: quantification of Col-1 and α-SMA in kidney tissues (Normalized to β-actin; $n = 6$). *I* and *J*: representative immunohistochemical staining and quantification of α-SMA in kidney tissues of mice (scale bar = 50 μm; $n = 6$). *K* and *L*: mRNA levels of fibrosis-associated genes including *Col1a* and *Acta2* in kidney tissues of mice (Normalized to WT-Sham group; $n = 6$). All quantitative data are presented as means ± SE; $^{*}P < 0.05$, $^{**}P < 0.01$, and $^{***}P < 0.001$. α-SMA, alpha-smooth muscle actin; Ang II, angiotensin II; BUN, blood urea nitrogen; Col-1, collagen 1; WT, wild type; *OTUD6A*$^{-/-}$, ovarian tumor domain-containing protein 6 A knockout.

significantly lower in *OTUD6A*$^{-/-}$ mice as compared with the WT mice (Fig. 2, *F–H*). Furthermore, immunohistochemical staining also confirmed that Ang II enhanced α-SMA level in kidney tissues, which was attenuated in *OTUD6A*$^{-/-}$ mice (Fig. 2, *I* and *J*). In addition, Ang II increased mRNA levels of fibrosis genes in kidney tissues, including Col1a and Acta2. Such induction was relieved in *OTUD6A*$^{-/-}$ mice (Fig. 2, *K* and *L*). Taken together, OTUD6A deficiency protected mice against Ang II-induced kidney fibrosis.

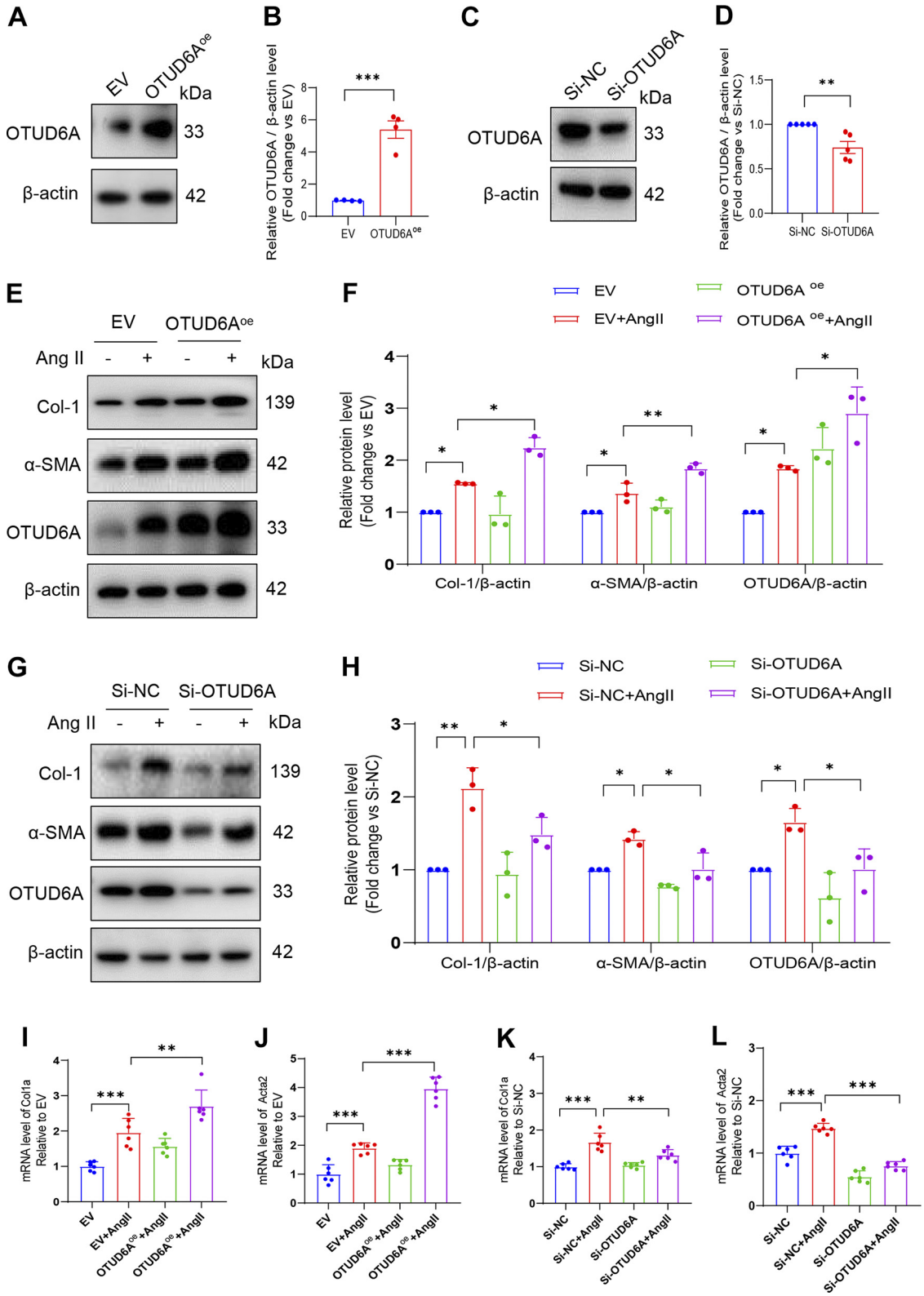

AJP-Cell Physiol • doi:10.1152/ajpcell.00394.2023 • www.ajpcell.org

OTUD6A Regulated Kidney Fibrotic Responses in NRK-52E Cells

To explore the role of OTUD6A in kidney remodeling, we enhanced OTUD6A level upon transfection with OTUD6A overexpression plasmid into NRK-52E cells (Fig. 3, *A* and *B*) and reduced OTUD6A level with siRNA transfection of NRK-52E cells (Fig. 3, *C* and *D*). The results further confirmed that Ang II-induced increase in the protein levels of fibrosis-associated factors, including Col-1 and α-SMA, which was further enhanced by OTUD6A overexpression (Fig. 3, *E* and *F*) but reduced upon transfection with OTUD6A siRNA (Fig. 3, *G* and *H*). The gene level of Col-1 and α-SMA followed a similar trend in NRK-52E cells (Fig. 3, *I*–*L*). These results showed that OTUD6A was essential in regulating Ang II-induced fibrosis in kidney tubular epithelial cells.

OTUD6A Inhibited K63-Linked Ubiquitination of STAT3 and Promoted STAT3 Activation

DUBs regulate protein degradation or function by deubiquitinating substrate proteins. We used immunoprecipitation along with mass spectrometry to confirm substrate proteins regulated by OTUD6A (Fig. 4*A*). Of the potential OTUD6A binding proteins, we identified five potential substrates for deubiquitination of OTUD6A. Given that STAT3 played a crucial role in modulating Ang II-induced hypertensive kidney injury and remodeling upon abnormal activation, and only STAT3 is restricted to kidney cells, we speculated that STAT3 might act as a candidate substrate of OTUD6A in regulating kidney remodeling (Fig. 4*B*; 25). Representative MS spectra of STAT3 were demonstrated in Fig. 4*C*. STAT3 is constitutively activated by phosphorylation of tyrosine 705 or serine 727 residues. Studies have confirmed rapid tyrosine 705 STAT3 phosphorylation in response to Ang II in NRK-52E cells, whereas serine 727 phosphorylation of STAT3 was not reported in kidney remodeling (25). Our results further confirmed that increased tyrosine 705 phosphorylated STAT3 expression was positively related to the tubular atrophy/interstitial fibrosis level in kidney tissues from patients with nephropathy (Fig. 4*D*; Supplemental Fig. S4; 16). To confirm the potential interaction between OTUD6A and STAT3, we transfected NIH/3T3 and NRK-52E cells with Flag-tagged OTUD6A. The results revealed that STAT3 interacted with OTUD6A in NIH/3T3 and NRK-52E cells (Fig. 4, *E* and *F*). Our results also revealed that OTUD6A immunoreactivity mainly colocalized to STAT3 in NRK-52E cells (Fig. 4*G*). We further found that the interaction of OTUD6A and STAT3 in kidney tissue was significantly enhanced under Ang II stimulation (Fig. 4*H*). More importantly, the ubiquitination of STAT3 was enhanced in Ang II-infused *OTUD6A*$^{-/-}$ mice as compared with the WT mice under Ang II stimulation, suggesting the in vivo deubiquitylation of STAT3 by OTUD6A (Fig. 4*I*). Furthermore, the immunofluorescence staining confirmed the colocalization of OTUD6A and STAT3 in kidney tissues (Supplemental Fig. S5).

To investigate the mechanism by which OTUD6A regulates STAT3 activity, we cotransfected STAT3 (His-tagged) and OTUD6A (Flag-tagged) plasmids in NIH/3T3 cells. The cells were exposed with carbobenzoxy-L-leucyl-L-leucyl-L-leucinal (MG132) to prevent proteasomal degradation of STAT3 protein. The results revealed that OTUD6A decreased the ubiquitination of STAT3 (Fig. 4*J*). To clarify the mechanism by which OTUD6A regulates STAT3 activity, we cotransfected STAT3 (His-tagged), OTUD6A (Flag-tagged), and mutated ubiquitin plasmids with only K48 and K63 active sites retained in NIH/3T3 cells. The cells were then exposed to MG132 to prevent proteasomal degradation of STAT3. The results indicated that the HA-K63 plasmid was sufficient to decrease the ubiquitination of STAT3 in the presence of OTUD6A at similar levels with HA-Ub (Fig. 4*K*). Our study identified a novel role for OTUD6A in activating STAT3 by inhibiting K63-linked ubiquitination.

OTUD6A Increased Ang II-Induced Kidney Fibrosis by Regulating STAT3 Phosphorylation

Regarding the interaction between OTUD6A and STAT3, we further explored whether OTUD6A modulates STAT3 in Ang II-induced kidney fibrosis. We observed increased Tyr705 p-STAT3 level following OTUD6A overexpression. However, the total STAT3 protein level was not affected (Fig. 5*A* and Supplemental Fig. S6). Thus, we hypothesized that OTUD6A enhanced the activation of Tyr705 p-STAT3.

We further upregulated OTUD6A in NRK-52E cells and exposed the cells to 1 μM Ang II for 1 h. OTUD6A overexpression in NRK-52E cells exacerbated Ang II-induced p-STAT3 expression without affecting the total STAT3 level (Fig. 5*B* and Supplemental Fig. S7). Conversely, OTUD6A knockdown abolished Ang II-induced p-STAT3 level in NRK-52E cells (Fig. 5*C* and Supplemental Fig. S8). These data showed that OTUD6A functionally targeted STAT3 phosphorylation. STAT3 activation is mainly mediated by phosphorylation and nuclear translocation. We then explored whether OTUD6A regulated STAT3 nuclear translocation. The results confirmed that STAT3 nuclear translocation was enhanced upon OTUD6A overexpression in NRK-52E cells, as confirmed by immunoblotting and immunostaining results (Fig. 5, *D* and *E*, and Supplemental Fig. S9).

Figure 3. OTUD6A regulated kidney fibrotic responses in NRK-52E cells. *A* and *B*: representative immunoblots and quantitative analysis of OTUD6A in NRK-52E cells transfected with OTUD6A overexpression plasmids (Normalized to β-actin; $n = 4$). *C* and *D*: representative immunoblots and quantitative analysis for OTUD6A in NRK-52E cells transfected with OTUD6A siRNA (Normalized to β-actin; $n = 5$). *E* and *F*: representative immunoblots and quantitative analysis of Col-1, α-SMA, and OTUD6A in NRK-52E cells transfected with OTUD6A overexpression plasmids and exposed with 1 μM Ang II (Normalized to β-actin; $n = 3$). *G* and *H*: representative immunoblots and quantitative analysis of OTUD6A, Col-1, and α-SMA in NRK-52E cells transfected with OTUD6A siRNA and exposed with 1 μM Ang II (Normalized to β-actin; $n = 3$). *I* and *J*: real-time quantitative polymerase chain reaction (qPCR) assay evaluating fibrosis-associated factors including col-1 and *Acta2* in NRK-52E cells transfected with OTUD6A overexpression plasmids and exposed with 1 μM Ang II (Normalized to the EV group; $n = 6$). *K* and *L*: real-time quantitative polymerase chain reaction (qPCR) assay evaluating fibrosis-associated factors including col-1 and *Acta2* in NRK-52E cells transfected with OTUD6A siRNA and exposed with 1 μM Ang II (Normalized to the Si-NC group; $n = 6$). Mean ± SE; $^{*}P < 0.05$, $^{**}P < 0.01$ and $^{***}P < 0.001$. α-SMA, alpha-smooth muscle actin; Ang II, angiotensin II; Col-1, collagen 1; EV, empty vector; NRK-52E, normal rat kidney-52E; OTUD6A^{oe}, ovarian tumor domain-containing protein 6 A overexpression; Si-NC, small interfering RNA-negative control; Si-OTUD6A, small interfering RNA-ovarian tumor domain-containing protein 6 A.

We then explored whether OTUD6A deficiency modulated STAT3 activation in kidney tissues of Ang II-infused mice. The results showed that Ang II elicited STAT3 phosphorylation in WT mice, which was further suppressed in *OTUD6A*$^{-/-}$ mice (Fig. 5, *F–H*). The immunohistochemistry also revealed reduced STAT3 phosphorylation in *OTUD6A*$^{-/-}$ mice (Fig. 5*I* and Supplemental Fig. S10). Finally, we explored whether STAT3 regulates OTUD6A during kidney metabolism. We challenged NRK-52E cells with Ang II in the presence or absence of STAT3 inhibitor stattic. Stattic selectively inhibits

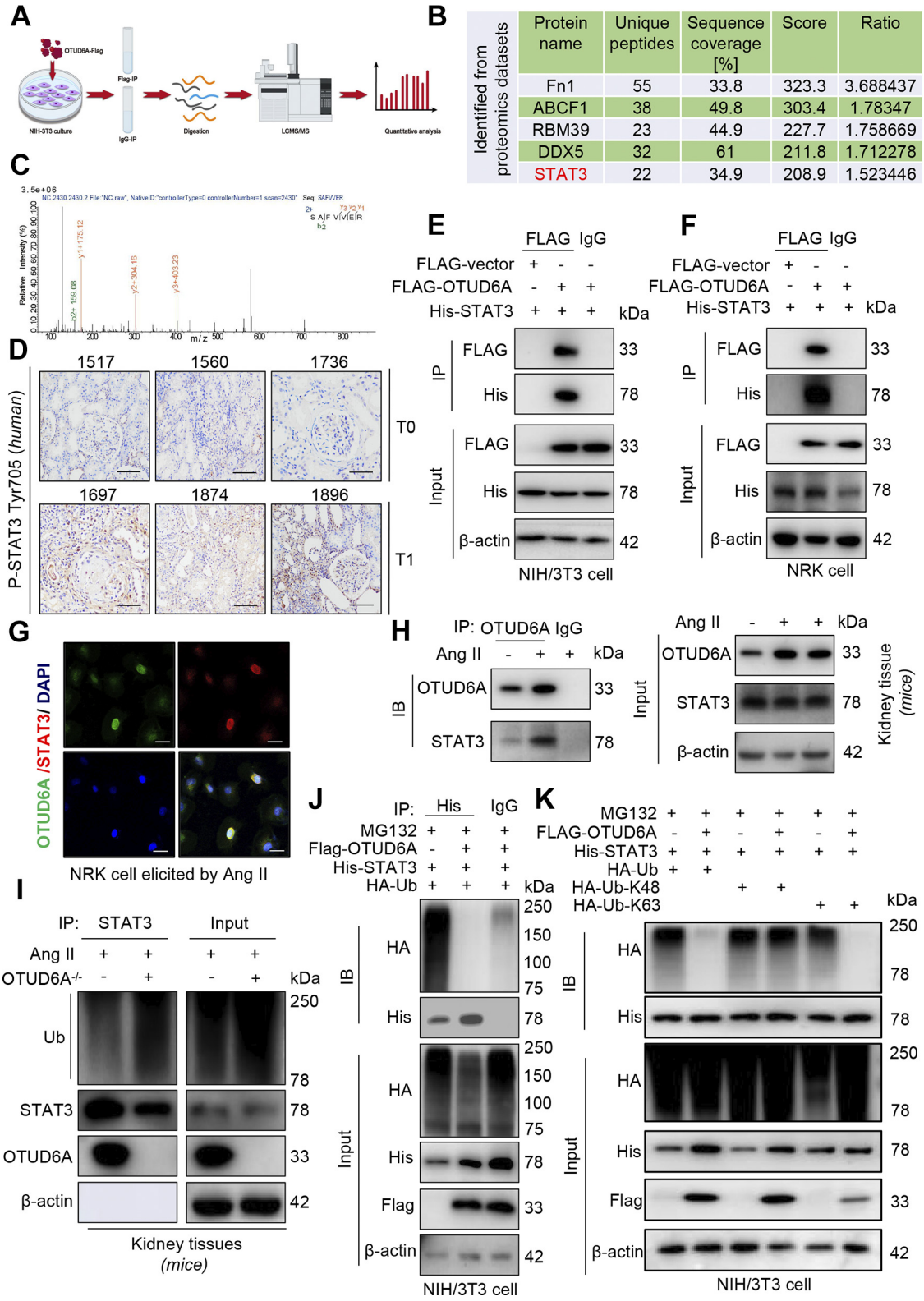

AJP-Cell Physiol • doi:10.1152/ajpcell.00394.2023 • www.ajpcell.org

activation and nuclear translocation of STAT3 (26, 27). The results revealed that stattic prevented p-STAT3 level in NRK-52E cells challenged with Ang II for 1 h without affecting the OTUD6A level (Fig. 5, *J* and *L*). Further, stattic reduced both protein and mRNA levels of Col-1 and α-SMA in NRK-52E cells upon Ang II exposure for 24 h without affecting the level of OTUD6A (Fig. 5, *K* and *M*, and Supplemental Fig. S11). Taken together, these results provided strong evidence that OTUD6A enhanced STAT3 Tyr-705 phosphorylation and nuclear translocation to regulate the kidney fibrosis. A schematic illustration of the main findings is shown in Fig. 6.

DISCUSSION

DUBs are proteases that regulate protein turnover and emerging therapeutic targets for various diseases (8). Although substantial evidence supported the importance of OTUD6A in tumor progression (14, 15), few studies have reported the role and function of OTUD6A in kidney fibrosis. For the first time, we revealed that OTUD6A was highly upregulated in the kidneys of patients with chronic kidney disease and Ang II-infused mice. *OTUD6A*$^{-/-}$ mice, when challenged with the same Ang II regimen, showed suppressed kidney dysfunction and fibrosis compared with the control mice. Mechanistically, OTUD6A coimmunoprecipitated and costained with STAT3. OTUD6A removed K63 ubiquitination to promote STAT3 phosphorylation and nuclear translocation. Moreover, OTUD6A deletion alleviated the aberrant profibrogenic factors in Ang II-stimulated tubular epithelial cells, whereas OTUD6A overexpression enhanced the fibrosis process. Thus, our findings established OTUD6A as a novel regulator of STAT3 in regulating kidney remodeling and highlighted OTUD6A as a potential therapeutic target for HKD.

Although almost 100 putative DUBs have been confirmed, research on DUBs in maladaptive kidney remolding remains scarce (8). Only recently, dysregulated DUBs, purely from the USP family, have been identified in various models of kidney injury. USP11, USP7, USP22, and USP28 were proven to promote kidney injury by promoting partial epithelial-to-mesenchymal transition and tubulointerstitial fibrosis (9, 10, 12, 28). Conversely, USP25 and USP9X showed protective effects against kidney diseases (11, 29). Drugs targeting USP30 are in clinical development for kidney disease (30). However, the role and majority of substrates regulated by DUBs remain elusive, impeding efforts to prioritize specific therapeutic targets for kidney injuries. OTUD6A belongs to the OTU family of DUBs, which was initially reported as an oncogene and proved to promote breast and prostate tumorigenesis via deubiquitinating TopBP1 and c-Myc (14, 15). Recently, one study revealed that OTUD6A promoted intestinal inflammation and colitis via NOD-like receptor thermal protein domain associated protein 3 (NLRP3) deubiquitylation (13). In the present study, our results showed increased expression of OTUD6A in both kidney tissues of mice after Ang II administration and in the kidney samples of patients with nephropathy.

Moreover, *OTUD6A*$^{-/-}$ mice were more resistant to Ang II-induced kidney injury than the WT mice, as reflected by reduced kidney dysfunction and fibrosis. The Ang II-induced hypertension in mice was at the same level in *OTUD6A*$^{-/-}$ mice as the WT mice, suggesting that the protective effect of OTUD6A deficiency is independent of regulating blood pressure. Furthermore, the in vitro studies in kidney tubular epithelial cells revealed consistent findings, as OTUD6A overexpression was responsible for upregulating Ang II-induced fibrotic factors, whereas OTUD6A knockdown attenuated Ang II-elicited fibrosis. These results suggest a novel role of OTUD6A in kidney remodeling.

STAT3 regulates various cellular and molecular activities. Existing studies have confirmed the negative role of dysregulated STAT3 activation in various kidney diseases (31, 32). However, therapeutic applications of small-molecule STAT3 inhibitors against kidney injury are still limited. Therefore, identifying the upstream regulatory protein of STAT3 and clarifying its regulatory mechanism in a particular pathology is of great clinical significance. Previous studies revealed that STAT3 activation by Ang II is independent of angiotensin II receptor type 1 (25). Other signaling pathways initiated by Ang II may convey STAT3 activation (21). The function and degradation of proteins depend mainly on the ubiquitylation and deubiquitylation status (8). However, researches on the ubiquitylation and deubiquitylation regulation of STAT3 were limited. Only a few studies reported that A20 regulated STAT3-driven antimicrobial signaling via modulating its ubiquitination (33), and USP28 deubiquitinated STAT3 in a K48-linked manner (12). The deubiquitylating enzymes that regulate STAT3 remain largely elusive. Our results revealed that STAT3 activation was enhanced in the kidney samples of patients with nephropathy and mice challenged with Ang II administration. Although the mechanisms of STAT3 activation in kidney dysfunction remain

Figure 4. OTUD6A interacted directly with STAT3 and promoted STAT3 activation through deubiquitylation. *A*: schematic illustration of quantitative proteomic screen to identify proteins binding to OTUD6A. *B*: five potential substrates for deubiquitination of OTUD6A from MS analysis. *C*: MS/MS spectrum of the peptide showing SAFVVER from STAT3. Single-letter abbreviations: S, Ser; A, Ala; F, Phe; V, Val; E, Glu; R, Arg; *m*/*z*, mass/charge ratio. *D*: representative immunohistochemical staining of p-STAT3 in kidney biopsy samples obtained from IgA patients with nephropathy of different tubular atrophy/interstitial fibrosis (T0 and T1) (scale bar = 25 μm). *E* and *F*: NIH/3T3 and NRK-52E cells were transfected with His-tagged STAT3 and Flag-tagged OTUD6A. Anti-STAT3 antibody was used for CO-IP. Levels of flag-tagged OTUD6A were detected by IB. Coimmunoprecipitation of OTUD6A and STAT3 in NIH/3T3 cells (*E*) and NRK-52 cells (*F*) ($n = 3$). *G*: immunofluorescent staining showing colocalization of OTUD6A and STAT3 in NRK-52E cells challenged with Ang II. Endogenous OTUD6A was immunoprecipitated by anti-OTUD6A antibody (scale bar = 20 μm). *H*: representative immunoblots of Co-IP of OTUD6A and STAT3 in kidney tissues from mice treated with Ang II (control = IgG; $n = 3$). *I*: ubiquitinated STAT3 was detected by immunoblotting to clarify the in vivo ubiquitination pattern of STAT3 regulated by OTUD6A ($n = 3$). *J*: NIH/3T3 cells were transfected with His-STAT3, HA-Ub, and Flag-OTUD6A. Cells were then exposed to MG132. Ubiquitinated STAT3 was detected by immunoblotting using an His-specific antibody (control = IgG; $n = 3$). *K*: immunoprecipitation of STAT3 in NIH/3T3 cells that cotransfected with overexpression plasmids of His-STAT3, HA-Ub, HA-K48, and HA-K63 and then subjected to MG132. Ubiquitinated STAT3 was detected by immunoblotting via using an His-specific antibody to clarify the ubiquitination pattern of STAT3 regulated by OTUD6A ($n = 3$). Ang II, angiotensin II; CO-IP, coimmunoprecipitation; IB, immunoblotting; MG132, carbobenzoxy-L-leucyl-L-leucyl-L-leucinal; NIH/3T3, mouse embryonic fibroblast cells; NRK cell, normal rat kidney epithelial cell; OTUD6A, ovarian tumor domain-containing protein 6 A; STAT3, signal transducer and activator of transcription 3; Ub, Ubiquitin. Figure created with BioRender.com and used with permission.

unclear, our present study confirmed that OTUD6A promoted STAT3 phosphorylation.

STAT3 belongs to the transcription factor family. Upon stimulation, cytoplasmic STAT3 is phosphorylated at Y705 or Y727 site (32). A previous study showed that Ang II-induced STAT3 phosphorylation at Y705 promotes pathological kidney remodeling (34, 35). Consistent with the previous studies, we identified increased levels of STAT3 Y705 phosphorylation in the kidneys from patients with nephropathy as compared with the healthy controls. More importantly,

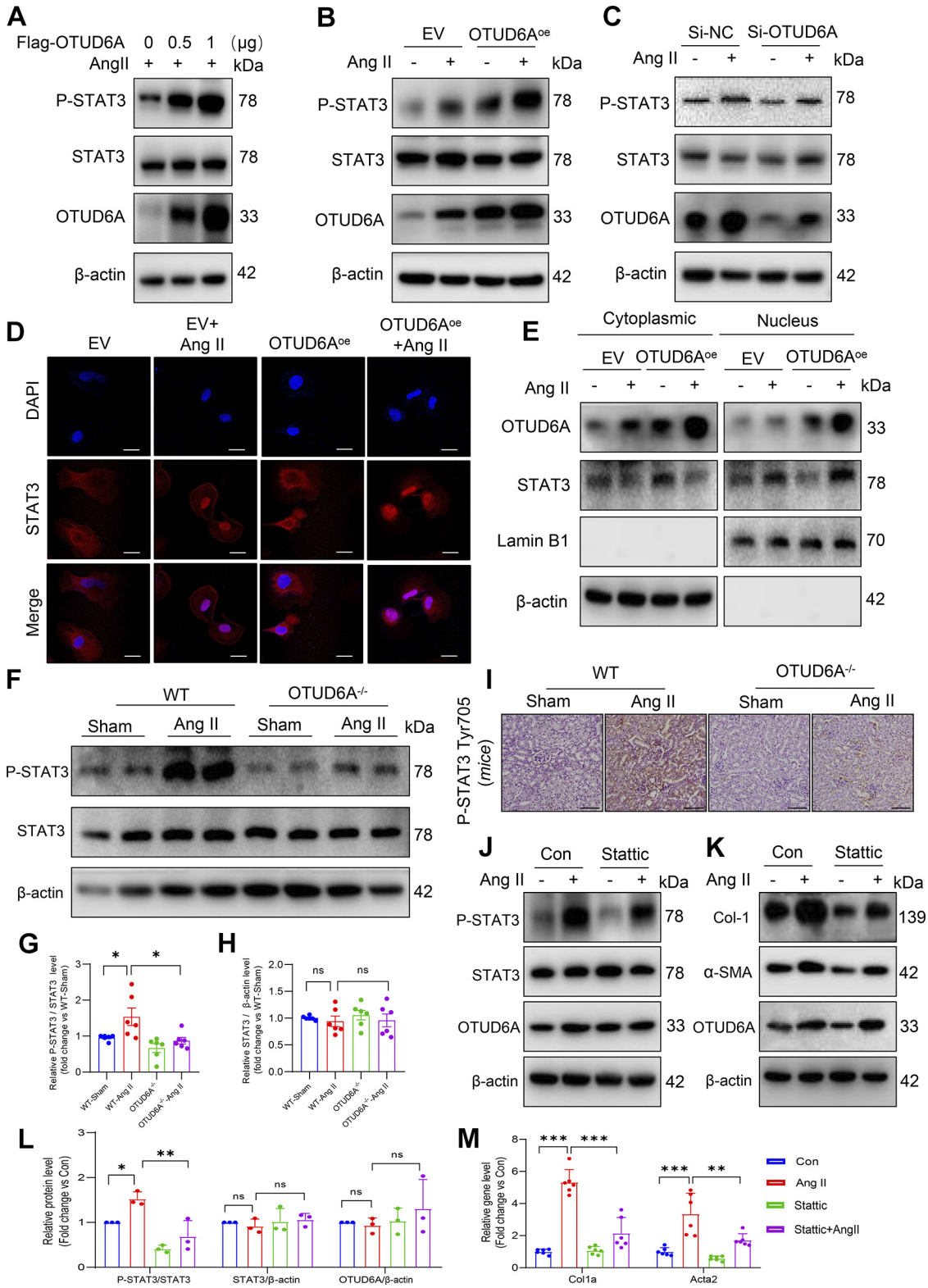

AJP-Cell Physiol • doi:10.1152/ajpcell.00394.2023 • www.ajpcell.org

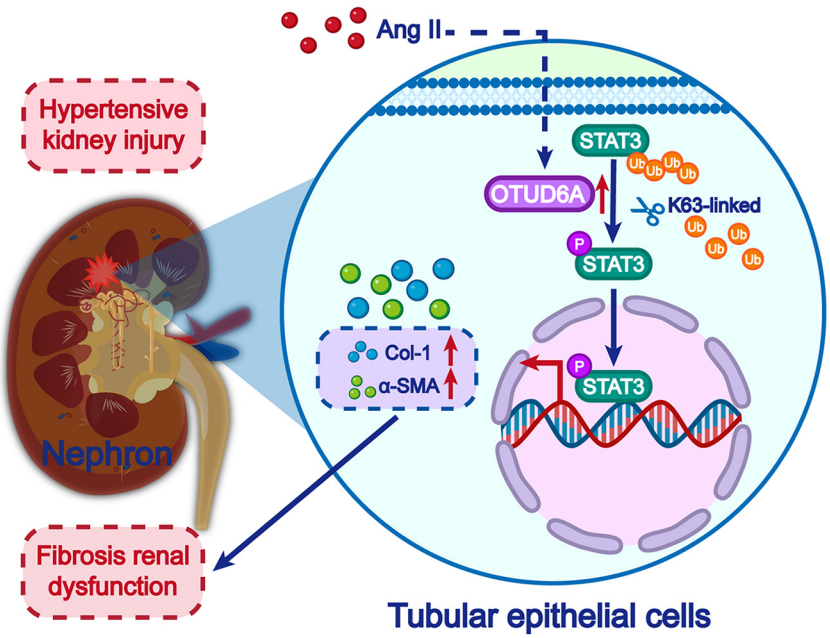

Figure 6. Schematic illustration for the role of OTUD6A on STAT3 during Ang II-induced kidney injury. STAT3 activity is normally kept in check by ubiquitination. OTUD6A deubiquitinates STAT3, thereby leading to STAT3 phosphorylation, nuclear translocation, and transcriptional activation of fibrosis-genes in the pathogenesis of Ang II-induced kidney injury. α-SMA, alpha-smooth muscle actin; Ang II, angiotensin II; Col-1, collagen 1; OTUD6A, ovarian tumor domain-containing protein 6 A; STAT3, signal transducer and activator of transcription 3.

OTUD6A detached K63-linked ubiquitination of STAT3 to promote STAT3 Y705 phosphorylation in NRK-52E cells. Taken together, our results indicated a new posttranscriptional modification of STAT3. Although our study identified STAT3 as an OTUD6A substrate, whether other substrates were regulated by OTUD6A in the process of kidney remodeling needs further exploration. Researches in cancer provide exciting possibilities. A study identified dynamin-related protein 1 (Drp1), a crucial regulator of mitochondrial fission and function, as a substrate of OTUD6A in colorectal cancer (36). More interestingly, Drp1 aggravated renal tubular epithelial cell apoptosis in kidney injury models (37). Furthermore, OTUD6A promoted intestinal inflammation and colitis through deubiquitylation of NLRP3 (13), which was proved to be closely related to kidney injury (38). Whether OTUD6A modulates Drp1 and NLRP3 involved in kidney remodeling needs further exploration.

Undeniably, our study has certain limitations. First, distinct cell populations, including tubular cells, mesangial cells, glomerular endothelial cells, podocytes, and immune cells play important roles in the kidney metabolism and disease progression (39). Although our results revealed that OTUD6A is mainly located in renal tubular epithelial cells, it is hard to exclude the contribution of OTUD6A in other kidney cell types in Ang II-induced renal fibrosis, which should be comprehensively explored in future studies. Second, STAT3, mainly expressed in kidney tubular epithelial cells, is also proved to regulate kidney cells such as mesangial cells and podocytes (40). Whether OTUD6A-STAT3 axis works in these cell types needs further exploration. Finally, no activator of OTUD6A is available at present. Mice should be injected with adeno-associated virus (AAV) 9-encoding OTUD6A vectors to further explore the in vivo regulatory role of OTUD6A-STAT3 signaling pathway.

Collectively, the results of our study suggested that OTUD6A played a pivotal role of in Ang II-induced kidney injury. OTUD6A deficiency remarkably protected mice against Ang II-induced kidney dysfunction and fibrosis. Mechanistically, OTUD6A bounded to STAT3 and removed K63 linked-ubiquitin chains to promote STAT3 phosphorylation and nuclear translocation, which then induced profibrotic gene transcription in epithelial cells. These studies

Figure 5. OTUD6A enhanced Ang II-induced kidney fibrosis by regulating STAT3 phosphorylation. *A*: representative immunoblots for p-STAT3 (Tyr-705), STAT3, and OTUD6A in NIH/3T3 cells transfected with different amount of Flag-OTUD6A overexpression plasmids under Ang II treatment ($n = 3$). *B*: representative immunoblots for p-STAT3 (Tyr-705), STAT3, and OTUD6A in NRK-52E cells transfected with OTUD6A overexpression plasmids and exposed to 1 μM Ang II for 1 h ($n = 3$). *C*: representative immunoblots for p-STAT3 (Tyr-705), STAT3, and OTUD6A in NRK-52E cells transfected with OTUD6A siRNA and exposed to 1 μM Ang II for 1 h ($n = 3$). *D*: immunofluorescence staining showing nuclear and cytoplasmic localization of STAT3 (red) in NRK-52E cells with various treatment. Cells were fixed and labelled with anti-STAT3 antibody. ($n = 3$, scale bar =25 μm). *E*: NRK-52E cells were transfected with OTUD6A-overexpressing vectors. Cells were then challenged with 1 μM Ang II for 1 h. Representative immunoblots of STAT3 and OTUD6A in cytosolic and nuclear fractions (Normalized to β-actin and Lamin B1; $n = 3$). *F–H*: representative immunoblots and quantitative analysis for p-STAT3 (Tyr-705) and STAT3 in kidney tissues from WT or *OTUD6A*$^{-/-}$ mice under Ang II treatment (Normalized to β-actin and Lamin B1) ($n = 6$). *I*: representative immunohistochemical staining image of p-STAT3 (Tyr-705) in kidney sections from WT or *OTUD6A*$^{-/-}$ mice under Ang II treatment. *J* and *L*: representative immunoblots and quantitative analysis for p-STAT3 (Tyr-705), STAT3, and OTUD6A expression in NRK-52 cells challenged with or without Ang II and/or STAT3 inhibitor Stattic (Normalized to β-actin and STAT3) ($n = 3$). *K*: representative immunoblots for Col-1, α-SMA, and OTUD6A expression in NRK-52 cells challenged with or without Ang II and/or STAT3 inhibitor Stattic. *M*: relative gene expression of Col-1 and α-SMA in NRK-52 cells challenged with or without STAT3 inhibitor Stattic under Ang II treatment (Normalized to the control group) ($n = 3$). All quantitative data is presented as means ± SE; Ns, not significant, $^{*}P < 0.05$, $^{**}P < 0.01$, $^{***}P < 0.001$. α-SMA, alpha-smooth muscle actin; Ang II, angiotensin II; Col-1, collagen 1; Con, control; EV, empty vector; NIH/3T3, mouse embryonic fibroblast cells; NRK-52E, normal rat kidney-52E; OTUD6A, ovarian tumor domain-containing protein 6 A; OTUD6A^{oe}, OTUD6A overexpression; p-STAT3, phosphorylated signal transducer and activator of transcription 3; Si-NC, Small interfering RNA-negative control; Si-OTUD6A, Small interfering RNA-OTUD6A; STAT3, signal transducer and activator of transcription 3.

identified STAT3 as a direct substrate of OTUD6A and indicated OTUD6A as a potential therapeutic target for HKD.

DATA AVAILABILITY

Data will be made available upon reasonable request.

SUPPLEMENTAL DATA

Supplemental Tables S1–S4 and Supplemental Figs. S1–S11: https://doi.org/10.6084/m9.figshare.24649044.

ACKNOWLEDGMENTS

The authors thank Professor Fuping You from Peking University for providing us with the whole body *OTUD6A*$^{-/-}$ mice in the C57BL/6J background. We are grateful to the patients who participated in this study.

GRANTS

This study was supported by the National Natural Science Foundation of China (81930108 to G.L.); Zhejiang Provincial Key Scientific Project (2021C03041 to G.L. and LY21H140003 to X.S.); and the Foundation for the new star of the medical industry in Zhejiang Province to X.S.

DISCLOSURES

No conflicts of interest, financial or otherwise, are declared by the authors.

AUTHOR CONTRIBUTIONS

G.C., S.H., and G.L. conceived and designed research; X.S., T.W., and Z.Z. performed experiments; J.H. and B.Y. analyzed data; S.C. and Z.F. interpreted results of experiments; S.C. and Y.Z. prepared figures; X.S. drafted manuscript; Y.Z. and W.L. edited and revised manuscript; G.C. and G.L. approved final version of manuscript.

REFERENCES

1. **Sanz AB**, **Sanchez-Niño MD**, **Ramos AM**, **Ortiz A.** Regulated cell death pathways in kidney disease. *Nat Rev Nephrol* 19: 281–299, 2023. doi:10.1038/s41581-023-00694-0.
2. **Ruiz-Ortega M**, **Rayego-Mateos S**, **Lamas S**, **Ortiz A**, **Rodrigues-Diez RR.** Targeting the progression of chronic kidney disease. *Nat Rev Nephrol* 16: 269–288, 2020. doi:10.1038/s41581-019-0248-y.
3. **Ruiz-Ortega M**, **Egido J.** Angiotensin II modulates cell growth-related events and synthesis of matrix proteins in renal interstitial fibroblasts. *Kidney Int* 52: 1497–1510, 1997. doi:10.1038/ki.1997.480.
4. **Cruz-López EO**, **Ye D**, **Wu C**, **Lu HS**, **Uijl E**, **Mirabito Colafella KM**, **Danser AHJ.** Angiotensinogen suppression: a new tool to treat cardiovascular and renal disease. *Hypertension* 79: 2115–2126, 2022. doi:10.1161/HYPERTENSIONAHA.122.18731.
5. **Kourtidou C**, **Tziomalos K.** The role of histone modifications in the pathogenesis of diabetic kidney disease. *IJMS* 24: 6007, 2023. doi:10.3390/ijms24066007.
6. **Osei-Amponsa V**, **Walters KJ.** Proteasome substrate receptors and their therapeutic potential. *Trends Biochem Sci* 47: 950–964, 2022. doi:10.1016/j.tibs.2022.06.006.
7. **Jin S-J**, **Kudo Y**, **Horiguchi T.** The role of deubiquitinating enzyme in head and neck squamous cell carcinoma. *IJMS* 24: 552, 2022. doi:10.3390/ijms24010552.
8. **Shen J-L**, **Lin X-N**, **Dai F-F**, **Chen G-L**, **Lin H-B**, **Fang B-J**, **Liu H.** Ubiquitin-specific peptidases: players in bone metabolism. *Cell Prolif* 56: e13444, 2023. doi:10.1111/cpr.13444.
9. **Dong B-Q**, **Ding C-G**, **Xiang H-L**, **Zheng J**, **Li X**, **Xue W-J**, **Li Y.** USP7 accelerates FMR1-mediated ferroptosis by facilitating TBK1 ubiquitination and DNMT1 deubiquitination after renal ischemia-reperfusion injury. *Inflamm Res* 71: 1519–1533, 2022. doi:10.1007/s00011-022-01648-1.
10. **Zhao X-L**, **He X-L**, **Wei W-T**, **Huang K-P.** USP22 aggravated diabetic renal tubulointerstitial fibrosis progression through deubiquitinating and stabilizing Snail1. *Eur J Pharmacol* 947: 175671, 2023. doi:10.1016/j.ejphar.2023.175671.
11. **Zhao Y**, **Chen X**, **Lin Y-M**, **Li Z-D**, **Su X**, **Fan S-J**, **Chen Y-H**, **Wang X**, **Liang G.** USP25 inhibits renal fibrosis by regulating TGFβ-SMAD signaling pathway in Ang II-induced hypertensive mice. *Biochim Biophys Acta Mol Basis Dis* 1869: 166713, 2023. doi:10.1016/j.bbadis.2023.166713.
12. **Ren Y**, **Zhu X-D**, **Fu K-Q**, **Zhang H-R**, **Zhao W-C**, **Lin Y**, **Fang Q**, **Wang J-Q**, **Chen Y-P**, **Guo D.** Inhibition of deubiquitinase USP28 attenuates cyst growth in autosomal dominant polycystic kidney disease. *Biochem Pharmacol* 207: 115355, 2023. doi:10.1016/j.bcp.2022.115355.
13. **Liu X**, **Fang Y**, **Lv X**, **Hu C**, **Chen G**, **Zhang L**, **Jin B**, **Huang L**, **Luo W**, **Liang G**, **Wang Y.** Deubiquitinase OTUD6A in macrophages promotes intestinal inflammation and colitis via deubiquitination of NLRP3. *Cell Death Differ* 30: 1457–1471, 2023. doi:10.1038/s41418-023-01148-7.
14. **Zhao Y**, **Huang X-P**, **Zhu D**, **Wei M**, **Luo J-C**, **Yu S-Y**, **Tian Y-L**, **Zheng X-F.** Deubiquitinase OTUD6A promotes breast cancer progression by increasing TopBP1 stability and rendering tumor cells resistant to DNA-damaging therapy. *Cell Death Differ* 29: 2531–2544, 2022. doi:10.1038/s41418-022-01036-6.
15. **Peng Y-H**, **Liu J**, **Wang Z**, **Cui C**, **Zhang T-T**, **Zhang S-X**, **Gao P-P**, **Hou Z-W**, **Liu H-D**, **Guo J-P**, **Zhang J-F**, **Wen Y-R**, **Wei W-Y**, **Zhang L-Q**, **Liu J-K**, **Long J-G.** Prostate-specific oncogene OTUD6A promotes prostatic tumorigenesis via deubiquitinating and stabilizing c-Myc. *Cell Death Differ* 29: 1730–1743, 2022. doi:10.1038/s41418-022-00960-x.
16. **Trimarchi H**, **Barratt J**, **Cattran DC**, **Cook HT**, **Coppo R**, **Haas M**, **Liu Z-H**, **Roberts IS**, **Yuzawa Y**, **Zhang H**, **Feehally J**; **Conference Participants.** Oxford classification of IgA nephropathy 2016: an update from the IgA nephropathy classification working group. *Kidney Int* 91: 1014–1021, 2017. doi:10.1016/j.kint.2017.02.003.
17. **Goodyear MD**, **Krleza-Jeric K**, **Lemmens T.** The Declaration of Helsinki. *BMJ* 335: 624–625, 2007. doi:10.1136/bmj.39339.610000.BE.
18. **Ye B-Z**, **Zhou H**, **Chen Y-H**, **Luo W**, **Lin W-T**, **Zhao Y**, **Han J-B**, **Han X**, **Huang W-J**, **Wu G-J**, **Wang X**, **Liang G.** USP25 ameliorates pathological cardiac hypertrophy by stabilizing SERCA2a in cardiomyocytes. *Circ Res* 132: 465–480, 2023. doi:10.1161/CIRCRESAHA.122.321849.
19. **Schindelin J**, **Arganda-Carreras I**, **Frise E**, **Kaynig V**, **Longair M**, **Pietzsch T**, **Preibisch S**, **Rueden C**, **Saalfeld S**, **Schmid B**, **Tinevez J-Y**, **White DJ**, **Hartenstein V**, **Eliceiri K**, **Tomancak P**, **Cardona A.** Fiji: an open-source platform for biological-image analysis. *Nat Methods* 9: 676–682, 2021. doi:10.1038/nmeth.2019.
20. **Hohl M**, **Selejan S-R**, **Wintrich J**, **Lehnert U**, **Speer T**, **Schneider C**, **Mauz M**, **Markwirth P**, **Wong DWL**, **Boor P**, **Kazakov A**, **Mollenhauer M**, **Linz B**, **Klinkhammer BM**, **Hübner U**, **Ukena C**, **Moellmann J**, **Lehrke M**, **Wagenpfeil S**, **Werner C**, **Linz D**, **Mahfoud F**, **Böhm M.** Renal denervation prevents atrial arrhythmogenic substrate development in CKD. *Circ Res* 130: 814–828, 2022. doi:10.1161/CIRCRESAHA.121.320104.
21. **Xu Z**, **Luo W**, **Chen L**, **Zhuang Z**, **Yang D**, **Qian J**, **Khan ZA**, **Guan X**, **Wang Y**, **Li X**, **Liang G.** Ang II (angiotensin II)-induced FGFR1 (fibroblast growth factor receptor 1) activation in tubular epithelial cells promotes hypertensive kidney fibrosis and injury. *Hypertension* 79: 2028–2041, 2022. doi:10.1161/HYPERTENSIONAHA.122.18657.
22. **Long L-Z**, **Zhang X-L**, **Wen Y**, **Li J-P**, **Wei L-H**, **Cheng Y**, **Liu H-X**, **Chu J-F**, **Fang Y**, **Xie Q-R**, **Shen A**, **Peng J.** Qingda granule attenuates angiotensin II-induced renal apoptosis and activation of the p53 pathway. *Front Pharmacol* 12: 770863, 2021. doi:10.3389/fphar.2021.770863.
23. **Miao N-J**, **Xie H-Y**, **Xu D**, **Yin J-Y**, **Wang Y-Z**, **Wang B**, **Yin F**, **Zhou Z-L**, **Cheng Q**, **Chen P-P**, **Zhou L**, **Xue H**, **Zhang W**, **Wang X-X**, **Liu J**, **Lu L-M.** Caspase-11 promotes renal fibrosis by stimulating IL-1β maturation via activating caspase-1. *Acta Pharmacol Sin* 40: 790–800, 2019. doi:10.1038/s41401-018-0177-5.
24. **Curran-Everett D**, **Benos DJ.** Guidelines for reporting statistics in journals published by the American Physiological Society. *Am J*

Physiol Heart Circ Physiol 287: H447–H449, 2004. doi:10.1152/ajpheart.00478.2004.

25. **Xu Z**, **Zou C-P**, **Yu W-H**, **Xu S-J**, **Huang L**, **Khan Z**, **Wang J-Y**, **Liang G**, **Wang Y.** Inhibition of STAT3 activation mediated by toll-like receptor 4 attenuates angiotensin II-induced renal fibrosis and dysfunction. *Br J Pharmacol* 178: 998, 2021]. doi:10.1111/bph.15374.
26. **Reich NC**, **Liu L.** Tracking STAT nuclear traffic. *Nat Rev Immunol* 6: 602–612, 2006. doi:10.1038/nri1885.
27. **Schust J**, **Sperl B**, **Hollis A**, **Mayer TU**, **Berg T.** Stattic: a small-molecule inhibitor of STAT3 activation and dimerization. *Chem Biol* 13: 1235–1242, 2006. doi:10.1016/j.chembiol.2006.09.018.
28. **Shi Y-F**, **Tao M**, **Chen H**, **Ma X-Y**, **Wang Y**, **Hu Y**, **Zhou X**, **Li J-Q**, **Cui B-B**, **Qiu A-D**, **Zhuang S-G**, **Liu N.** Ubiquitin-specific protease 11 promotes partial epithelial-to-mesenchymal transition by deubiquitinating the epidermal growth factor receptor during kidney fibrosis. *Kidney Int* 103: 544–564, 2023. doi:10.1016/j.kint.2022.11.027.
29. **Sun X-H**, **Xiao H-M**, **Zhang M**, **Lin Z-Y**, **Yang Y**, **Chen R**, **Liu P-Q**, **Huang K-P**, **Huang H-Q.** USP9X deubiquitinates connexin43 to prevent high glucose-induced epithelial-to-mesenchymal transition in NRK-52E cells. *Biochem Pharmacol* 188: 114562, 2021. doi:10.1016/j.bcp.2021.114562.
30. **Doherty LM**, **Mills CE**, **Boswell SA**, **Liu X-X**, **Hoyt CT**, **Gyori B**, **Buhrlage SJ**, **Sorger PK.** Integrating multi-omics data reveals function and therapeutic potential of deubiquitinating enzymes. *eLife* 11: e72879, 2022. doi:10.7554/eLife.72879.
31. **Pace J**, **Paladugu P**, **Das B**, **He J-C**, **Mallipattu SK.** Targeting STAT3 signaling in kidney disease. *Am J Physiol Renal Physiol* 316: F1151–F1161, 2019. doi:10.1152/ajprenal.00034.2019.
32. **Cai H**, **Chen Y**, **Feng Y**, **Asadi M**, **Kaufman L**, **Lee K**, **Kehrer T**, **Miorin L**, **Garcia-Sastre A**, **Gusella GL**, **Gu L-Y**, **Ni Z-H**, **Mou S**, **He JC**, **Zhou W-B.** SARS-CoV-2 viral protein ORF3A injures renal tubules by interacting with TRIM59 to induce STAT3 activation. *Mol Ther* 31: 774–787, 2023. doi:10.1016/j.ymthe.2022.12.008.
33. **Liu X-Y**, **Mao Y**, **Kang Y-H**, **He L**, **Zhu B**, **Zhang W**, **Lu Y**, **Wu Q-N**, **Xu D-K**, **Shi L-Y.** MicroRNA-127 promotes anti-microbial host defense through restricting A20-mediated de-ubiquitination of STAT3. *iScience* 23: 100763, 2020. doi:10.1016/j.isci.2019.100763.
34. **Ye S-J**, **Luo W**, **Khan ZA**, **Wu G-J**, **Xuan L-N**, **Shan P-R**, **Lin K**, **Chen T-W**, **Wang J-Y**, **Hu X**, **Wang S-J**, **Huang W-J**, **Liang G.** Celastrol attenuates angiotensin II-induced cardiac remodeling by targeting STAT3. *Circ Res* 130: e2, 2022. doi:10.1161/RES.0000000000000532.
35. **Kurdi M**, **Booz GW.** Can the protective actions of JAK-STAT in the heart be exploited therapeutically? Parsing the regulation of interleukin-6-type cytokine signaling. *J Cardiovasc Pharmacol* 50: 126–141, 2007. doi:10.1097/FJC.0b013e318068dd49.
36. **Shi L**, **Liu J**, **Peng Y-H**, **Zhang J-F**, **Dai X-P**, **Zhang S-X**, **Wang Y-Y**, **Liu J-K**, **Long J-G.** Deubiquitinase OTUD6A promotes proliferation of cancer cells via regulating Drp1 stability and mitochondrial fission. *Mol Oncol* 14: 3169–3183, 2020. doi:10.1002/1878-0261.12825.
37. **Cleveland KH**, **Schnellmann RG.** The β(2)-adrenergic receptor agonist formoterol restores mitochondrial homeostasis in glucose-induced renal proximal tubule injury through separate integrated pathways. *Biochem Pharmacol* 209: 115436, 2023. doi:10.1016/j.bcp.2023.115436.
38. **Wu M**, **Ma Y-W**, **Chen X-T**, **Liang N**, **Qu S**, **Chen H-B.** Hyperuricemia causes kidney damage by promoting autophagy and NLRP3-mediated inflammation in rats with urate oxidase deficiency. *Dis Model Mech* 14: dmm048041, 2021. doi:10.1242/dmm.048041.
39. **Fu J**, **Akat KM**, **Sun Z-G**, **Zhang W-J**, **Schlondorff D**, **Liu Z-H**, **Tuschl T**, **Lee K**, **He JC.** Single-cell RNA profiling of glomerular cells shows dynamic changes in experimental diabetic kidney disease. *J Am Soc Nephrol* 30: 533–545, 2019. doi:10.1681/ASN.2018090896.
40. **Zhou J**, **Yang J**, **Wang Y-M**, **Ding H**, **Li T-S**, **Liu Z-H**, **Chen L**, **Jiao R-Q**, **Zhang D-M**, **Kong LD.** IL-6/STAT3 signaling activation exacerbates high fructose-induced podocyte hypertrophy by ketohexokinase-A-mediated tristetraprolin down-regulation. *Cell Signal* 86: 110082, 2021. doi:10.1016/j.cellsig.2021.110082.